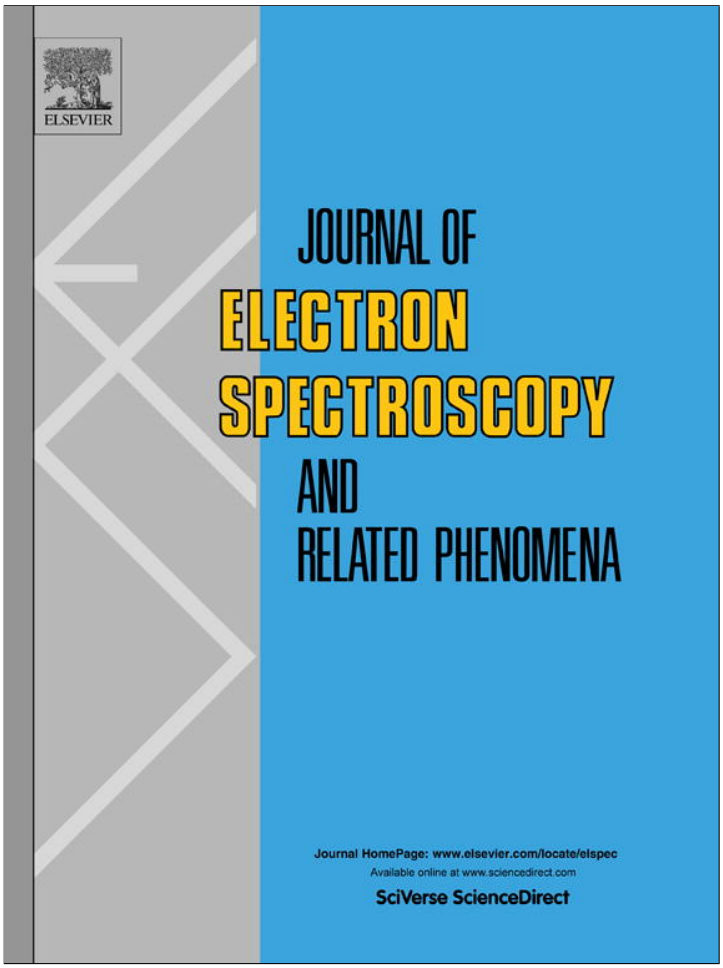

(This is a sample cover image for this issue. The actual cover is not yet available at this time.)

Journal of Electron Spectroscopy and Related Phenomena 185 (2012) 159–166

Contents lists available at SciVerse ScienceDirect

Journal of Electron Spectroscopy and Related Phenomena

journal homepage: www.elsevier.com/locate/elspec

Use of oxygen/nickel ratios in the XPS characterisation of oxide phases on nickel metal and nickel alloy surfaces

B.P. Payne[a], M.C. Biesinger[b], N.S. McIntyre[a,*]

[a] Department of Chemistry, The University of Western Ontario, London, ON N6A 5B7, Canada
[b] Surface Science Western, The University of Western Ontario, London, ON N6A 5B7, Canada

ARTICLE INFO

Article history:
Received 28 March 2011
Received in revised form 19 June 2012
Accepted 19 June 2012
Available online xxx

Keywords:
XPS
Ni oxides
Atomic ratios
Mixed phase oxides

ABSTRACT

The O/Ni ratios derived from the X-ray photoelectron (XP) spectra of a number of well-characterised Ni oxides were calculated and found to correspond well to the expected O/Ni ratios for these oxides. The measured ratios, combined with the characteristic XP spectra, provide a higher level of confidence to the assignment of O 1s chemical species, particularly for surfaces with multiple phases present. As examples of this, we discuss the additional information imparted by O/Ni ratios measured for oxides that were electrochemically grown on Ni and NiCr-20% alloy surfaces.

1. Introduction

X-ray photoelectron spectroscopy has extensively been used to study the oxidation and corrosion products formed on surfaces of Ni metal and its alloys [1–17]; the technique has provided chemical information about the oxides produced that is generally not available elsewhere. The information depth available (~5 nm) is sufficient to allow oxide structures and growth rates to be followed to a considerable length. While XPS chemical shifts have been useful in separating oxidic phases from the base alloy, clear identification of specific structures has been lacking because of complex Ni 2p line shapes and a large number of contributing sources to the O 1s spectra [13–17]. In the past, our laboratory has produced evidence for unique Ni $2p_{3/2}$ and O 1s spectra for polycrystalline NiO, β-$Ni(OH)_2$, and γ-NiOOH [1,4,18], including evidence for the presence of Ni^{3+} and defective O species, and have used this information to follow the oxide growth structures on Ni metal during reaction with O_2 gas [3] and H_2O vapour [2].

The Ni $2p_{3/2}$ and O 1s line shapes for single crystal NiO have been extensively studied by other authors resulting in a number of different peak assignments. The group of Sawatzky et al. studied the Ni $2p_{3/2}$ and O 1s spectra of a number of single crystal NiO (1 0 0) films ranging in thickness from 1 to 20 ML [19]. Over the course of this work an increase in the high BE shoulder of the Ni $2p_{3/2}$ spectra was observed with increasing film thickness. The increase in signal intensity was attributed to screening interactions arising from the donation of electrons to Ni^{2+} centres by O^{2-} anions situated around neighbouring cations. Analysis of the corresponding O 1s spectra showed the presence of only one oxidic peak, which they assigned to O^{2-} in NiO. The origin of the NiO doublet structure was further investigated by Sawatzky and co-workers using NiO as a dopant in MgO [20]. Again they observed a change in the intensity of the high BE peak in the doublet structure of the Ni 2p spectrum as the concentration of NiO was increased in a $Ni_xMg_{1-x}O$ crystal. When the Ni_x contribution was 0.4 or less very little intensity in the high BE component of the doublet structure was observed.

The line shape of NiO was also examined by Goodman et al. [21]. This group studied changes to the Ni $2p_{3/2}$ spectrum following the growth of single crystal MgO (1 0 0) films on single crystal NiO (1 0 0) substrates. Their work revealed BE shifts as high as 1.0 eV in both the Ni $2p_{3/2}$ and O 1s spectra with increasing MgO thickness. These BE shifts were attributed to the transfer of negative charge from the MgO film to the NiO substrate. In a subsequent publication Goodman and co-workers suggested that these shifts were more likely attributed to surface relaxation effects arising from small changes in the atomic organisation at the surface [22].

A number of studies monitoring the role of surface defects on the adsorption of gases on single crystal NiO (1 0 0) films were completed by Freund and several co-workers. Prior to any gas exposures Freund et al. studied the surface of a NiO (1 0 0) film grown on a Ni (1 0 0) substrate [23]. Analysis of the O 1s spectrum revealed two peaks; one attributed to O^{2-}, and a second assigned to either an OH or an O^- defect species shifted 1.4 eV to higher BE. This high BE species was found to be surface dependent using ARXPS and could

* Corresponding author. Tel.: +1 519 661 2111x86703.
E-mail address: smcintyr@uwo.ca (N.S. McIntyre).

0368-2048/$ – see front matter © 2012 Elsevier B.V. All rights reserved.
http://dx.doi.org/10.1016/j.elspec.2012.06.008

not be completely removed by heating. There was no conclusive spectral evidence to support the presence of significant levels of Ni^{3+} in the corresponding Ni $2p_{3/2}$ spectrum. In subsequent publications, Freund et al. concluded that the OH groups would bind at defect sites, giving rise to a peak at 531.4 eV in the O 1 s spectrum [24,25]. Using ARXPS it was also determined that the OH groups were located at the near surface, while heating of the film to temperatures above 327 °C resulted in a loss of the signal at 531.4 eV. The latter result was attributed to the loss of OH groups. Sputtering NiO (1 0 0) surfaces was also found to reduce some Ni^{2+} species to metallic Ni atoms. Subsequent exposure of these sputtered surfaces to O_2 followed by reaction with H_2O resulted in a larger high BE peak at 531.4 eV, a peak that could not be removed by heating without destroying the sample.

The effects of introducing defects into NiO films using ion sputtering were also examined by Freund et al. In this work ion bombardment of vacuum cleaved NiO (1 0 0) surface resulted in an increase in the intensity of the high BE peak of the characteristic Ni $2p_{3/2}$ doublet structure component [26]. This increase in intensity was attributed to the sputter induced formation of Ni^{3+} species. Using ARXPS it was determined that this species was located at the near surface. An increase in the Ni metal signal due to Ni^{2+} reduction was also observed with sputtering. Analysis of the corresponding O 1s spectrum with sputtering time showed only 1 peak. Freund et al. concluded that the presence of Ni^{3+} in the Ni 2p spectrum was not accompanied by a corresponding peak in the O 1s spectrum. They did however go on to suggest that defects sites on NiO surfaces are where H_2O molecules will adsorb.

Langell et al. monitored changes in the O 1s and Ni $2p_{3/2}$ spectra for NiO (1 1 1) films following O_2 gas exposures. Analysis of the O 1s spectra revealed two main peaks centred at 529.4 eV and 531.2, which they assigned to lattice O^{2-} and adsorbed OH groups [27,28]. The analysis of the corresponding Ni $2p_{3/2}$ spectra yielded no signals from Ni^{3+}. Heating of the NiO films resulted in a decrease in the intensity of the adsorbed OH component and at temperatures above 330 °C this peak could not be observed. In addition, a decrease in the O^{2-} peak intensity was also observed above this temperature.

Over the course of this work, it was found that most of the O/Ni atomic ratios, corrected for cross-section, energy and contributions from contaminants, appeared to provide a reliable measure of the actual atomic ratios. In the past other authors have occasionally used atomic ratios to determine the nature of the oxides formed on metallic surfaces exposed to O_2 and H_2O vapour [29,30]. Such measurements, if accurate could certainly provide additional information on the nature of the surface structures. For this reason, we have made additional O/Ni measurements of new- and previously acquired spectra of NiO [2], β-$Ni(OH)_2$ [2], γ-NiOOH [18], and $NiCr_2O_4$ [31] and have used these reference results to determine the ratios for oxide structures on Ni metal and NiCr-20% (NiCr) alloy surfaces that had undergone electrochemical oxidation. The O/Ni measurements on the unknown electrochemically treated surfaces correspond well with analyses of the standard O 1s and Ni $2p_{3/2}$ spectral line shapes.

2. Experimental

All XPS analyses were carried out with a Kratos Axis Ultra spectrometer using a monochromatic Al Kα (15 mA, 14 kV) X-ray source. The work function and the dispersion of the instrument were calibrated to give metallic Au $4f_{7/2}$ and Cu $2p_{3/2}$ signals of 83.95 eV and 932.63 eV, respectively. Differential surface charging was minimised using the Kratos charge neutraliser system with a filament current set between 1.7 and 1.9 A, and a charge balance ranging from 2.4 to 3.1 V. All XPS spectra were collected using the hybrid-focusing lens, a scan time of 180 s, and an analysis area of 700 μm × 300 μm. The survey spectra were obtained at a pass energy of 160 eV, a 0.7 eV energy step, over a binding energy (BE) range of 1100–0 eV. Analyses of the Ni 2p, Cr 2p, O 1s, and C 1s envelopes were carried out at pass energies of 10/20 eV, an energy step size of 0.05 eV, at energy ranges of 895–848 eV (30–40 sweeps), 595–570 (30 sweeps), 540–520 eV (15–20 sweeps), and 295–275 eV (10–20 sweeps), respectively. The base pressure of the analytical chamber during sample analysis was near 5×10^{-9} Torr.

Powder samples of polycrystalline NiO (99.998% pure, Puratronic) and β-$Ni(OH)_2$ (61% Ni) were obtained from Alfa Aesar (Ward Hill, MA, USA). The NiO powder was received in a sealed container and two samples were introduced to the spectrometer through an Ar filled glove box. Two additional NiO samples were exposed to air prior to X-ray analysis. The purity of the NiO powder was confirmed using both X-ray diffraction (XRD) and energy dispersive X-ray analysis (EDX), while the purity of the β-$Ni(OH)_2$ powder was confirmed solely by EDX [4]. The γ-NiOOH sample was originally obtained from Inco Limited and its characterisation has been previously reported [18]. The β-$Ni(OH)_2$ and γ-NiOOH powders were both loaded into the spectrometer from the air. The $NiCr_2O_4$ powder (90% pure) was obtained from Alfa Aesar and was exposed to the air prior to X-ray analysis [31]. All powder samples were either mounted onto a double-sided non-conductive polyethylene polymer or pressed into indium foil prior to X-ray exposure to further minimise spectral broadening due to charging. A polycrystalline Ni metal disk approximately 3.4 mm thick was cut from a metal rod (99.995% pure) purchased from Alfa Aesar. A similar sized disc of NiCr alloy manufactured by ACI Alloys Inc. (San Jose, CA, USA) was also studied. Both metallic samples were mechanically polished to a mirror finish using 0.05 μm γ-Al_2O_3 paste, sonicated in methanol for 20 min, and cathodically cleaned for 1 h at a constant potential of −1.5 V versus a 0.1 M Ag/AgCl reference electrode. Following surface reduction the metal disks were then subjected to aqueous corrosion for 3 h at a constant potential of 1.5 V versus the same reference electrode in a sealed autoclave at temperatures of 150 °C for Ni metal and 25 °C for the NiCr alloy. The electrolyte used was a 0.0001 M LiOH solution (pH = 10 at 25 °C) prepared in de-ionised H_2O.

CasaXPS Version 2.3.15 was used to analyse all XPS spectra collected as part of this work [32]. The background for all survey and high-resolution spectra was removed using a standard Shirley baseline [32]. The elemental concentration in atomic % (at.%) for all samples was determined from the analysis of XPS survey spectra using Wagner relative sensitivity factors (RSFs) specifically modified for analysing data obtained from a Kratos Axis Ultra spectrometer [32–34]. The Ni atomic concentrations presented in Table 1 were calculated using the area of Ni $2p_{3/2}$ region only. Previous publications by this group have used the same data analysis methods [2,3,35]. Analysis of the Ni $2p_{3/2}$ and Cr $2p_{3/2}$ spectra were completed using the fits previously published for polycrystalline NiO, β-$Ni(OH)_2$, γ-NiOOH, Cr_2O_3, $Cr(OH)_3{\cdot}xH_2O$ and $NiCr_2O_4$ [1,4,18–31,35]. Gaussian–Lorentzian line shapes of 50% (GL(50)) were found to be best for fitting the O 1s spectra, while the C 1s envelopes were best fitted with a 30% Lorentzian (GL(30)) contribution in the mixture.

All samples studied as a part of this work were determined to contain small amounts of adventitious C. Analyses of the high-resolution C 1s spectra showed a strong hydrocarbon line (C—C, C—H), which was used for spectral calibration and corrected to a BE of 284.8 ± 0.1 eV. Additional contributions from alcohol/ether (—COH, —COC—, O═C(O—C*)), carbonyl (—C═O), and ester (O═CO—) organic functional groups were also observed at average BEs of 286.1 ± 0.2 eV, 287.8 ± 0.2 eV, and 288.7 ± 0.2 eV, respectively. The (*) denotes the atom giving rise to the signal. Contamination of the O 1s line shape from O-containing adventitious C was corrected as described in earlier publications and was modelled

Table 1
Summary of the O 1s peak fitting results for the O^{2-}, O def, OH^- and interstitial H_2O species.

Sample	O^{2-}			O def			OH^-			Interstitial H_2O		
	BE (eV)	FWHM (eV)	Area (%)	BE (eV)	FWHM (eV)	Area (%)	BE (eV)	FWHM (eV)	Area (%)	BE (eV)	FWHM (eV)	Area (%)
NiO-1	529.3	0.90	68	531.1	1.32	27						
NiO-2	529.3	0.91	71	531.1	1.24	23						
NiO-3	529.4	0.94	69	530.9	1.30	20						
NiO-4	529.4	0.94	71	530.9	1.20	18						
$Ni(OH)_2$-1							530.8	1.30	95			
$Ni(OH)_2$-2							530.9	1.25	71	531.5	1.20	22
$Ni(OH)_2$-3							531.0	1.47	97			
$Ni(OH)_2$-4							531.2	1.41	93			
$Ni(OH)_2$-5							531.2	1.39	93			
γ-NiOOH	529.5	0.95	37				531.2	1.59	52			
$NiCr_2O_4$-1	529.9	1.02	77							531.2	1.52	20
$NiCr_2O_4$-2	530.0	0.97	82							531.2	1.25	15
Ni metal	529.2	1.00	23				531.1	1.34	51	531.7	1.20	13
NiCr metal												
Ni oxides	529.3	1.10	3.7				531.2	1.60	24	531.8[a]	1.28	7.2
Cr oxides	529.5[b]	1.10	6.4				531.3	1.56	30	530.2[d]	1.28	9.0
	530.0[c]		2.9									

[a] The observed BE shift for the interstitial H_2O species associated with $Ni(OH)_2$.
[b] The observed BE shift for the O^{2-} species bound in Cr_2O_3.
[c] The observed BE shift for the O^{2-} species bound in the Cr^{6+}-containing oxide.
[d] The observed BE shift for the interstitial H_2O species associated with $Cr(OH)_3$.

using five peaks representing O*═CO— (531.7 ± 0.2 eV), —C═O (532.0 ± 0.2 eV), —COC— (532.2 ± 0.2 eV), —COH (532.5 ± 0.2 eV), and O═CO*— (532.9 ± 0.2 eV) O species [2,35,36].

The relative atomic concentrations for the different Ni, Cr, O, and C species were determined using methods described in previous publications [2,35]. The error in the resultant O/M (M = Ni or Cr) ratios was estimated to be 10% (2 standard deviations). The CasaXPS software also allows for the normalised atomic ratios to be calculated directly from the high-resolution spectra using the "Standard Comps Report" button found under the "Report Spectra" tab in the "Quantification Window" [32]. However, during the course of this work O/Ni ratios calculated using this method were found to deviate significantly from what was stoichiometrically expected. In a previous publication by this group the O/Cr ratios for a number of Cr oxides were calculated [35]. When these ratios were modelled using the "Standard Comps Report" function the same O/Cr ratios were observed. It appears that this method works for systems containing Cr and O because the two peaks used for analysis (Cr $2p_{3/2}$ and O 1s) are only separated in kinetic energy (KE) by approximately 50 eV, while the difference between the Ni $2p_{3/2}$ and O 1s peaks is greater than 300 eV. As a result any calculation of atomic concentrations for Ni should be completed using the survey spectra (pass energy 160 eV) and not the high-resolution spectra.

3. Results and discussion

3.1. Polycrystalline NiO, β-Ni(OH)$_2$, γ-NiOOH, and $NiCr_2O_4$ samples

Representative high-resolution Ni $2p_{3/2}$ and O 1s spectra for NiO, β-$Ni(OH)_2$, γ-NiOOH, and $NiCr_2O_4$ are shown in Figs. 1–4. All Ni $2p_{3/2}$ and Cr $2p_{3/2}$ envelopes were modelled using the fits tabulated in Refs. [1,4,18–31,35]. The M $2p_{3/2}$ spectra of these compounds have been well characterised previously and were included solely as a reference for the corresponding O 1s spectra. For each O 1s spectrum, it was necessary to determine if each spectral component was associated intimately with the oxide structure or was associated with an ancillary phase such as organic contamination, or interstitial H_2O molecules.

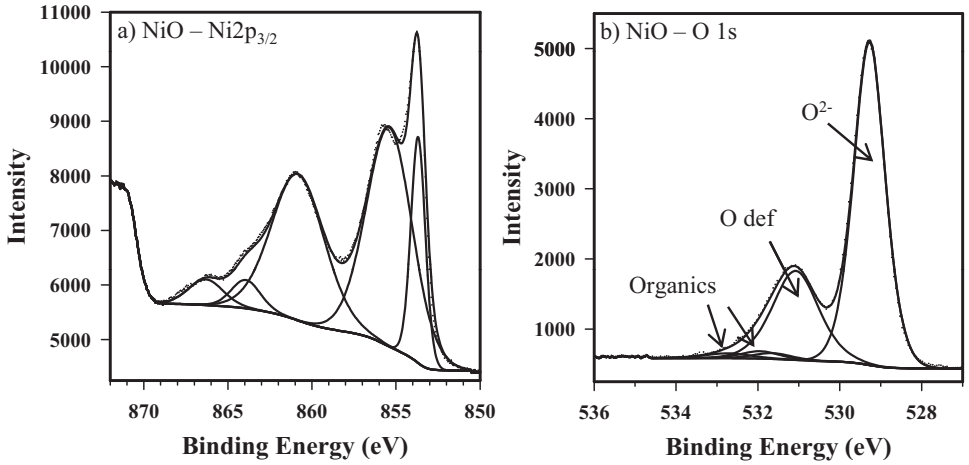

Fig. 1. Fitted high-resolution (a) Ni $2p_{3/2}$ and (b) O 1s spectra from a polycrystalline NiO powder loaded into the spectrometer through an Ar filled glove box. The Ni $2p_{3/2}$ spectrum was fit using the empirical peak fit for NiO tabulated in Ref. [4]. The O 1s spectrum has been fit with contributions from O^{2-} and O def. species. The remaining spectral intensity was assigned to organic contamination.

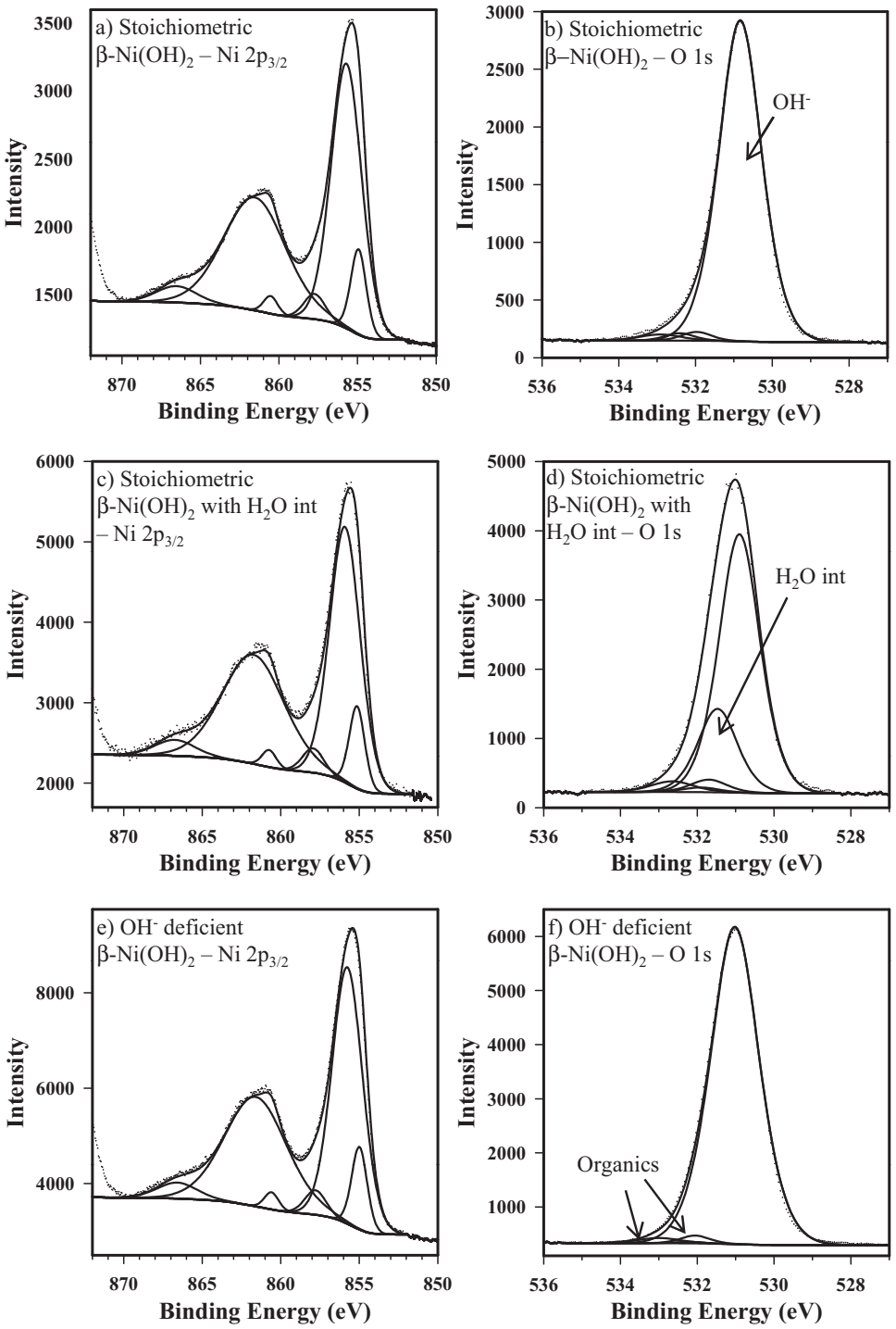

Fig. 2. Fitted high-resolution Ni $2p_{3/2}$ and O 1s spectra collected from three β-Ni(OH)$_2$ samples. The spectra illustrate the Ni $2p_{3/2}$ and O 1s line shapes for (a) and (b) stoichiometric β-Ni(OH)$_2$, (c) and (d) stoichiometric β-Ni(OH)$_2$ containing interstitial H_2O (H_2O int) within the brucite lattice, and (e) and (f) OH− deficient β-Ni(OH)$_2$. The Ni $2p_{3/2}$ spectra were fit using the empirical peak fit for β-Ni(OH)$_2$ tabulated in Ref. [4].

Representative high-resolution Ni $2p_{3/2}$ and O 1s spectra for polycrystalline NiO powder are shown in Fig. 1. The O 1s spectra for all NiO samples contained the well recognised lattice oxide peak (O^{2-}) with centroids that could be fitted to 529.3 eV or 529.4 eV depending on the sample (see Table 1). In addition, a higher BE peak was observed at either 531.1 eV or 530.9 eV; this has been previously attributed by us to oxygen atoms adjacent to Ni vacancies and thus deemed to be 'defective oxygen' (O def) [2]. A more convincing explanation for this peak has been provided by through the Nuclear Microprobe studies of Norton et al. [9] who provided evidence associating this peak with a hydride form of the oxide $NiO_1H_{0.2}$. The summed intensities of these peaks were used in the compilation of the O/Ni ratios for NiO shown in Table 2. All additional intensity in the O 1s spectra for NiO could be attributed to organic components present; thus no additional contributions from interstitial H_2O was found in any of the NiO examples studied (see below). Table 2 shows that, for NiO, the O/Ni ratios obtained are close to 1.0, within experimental error.

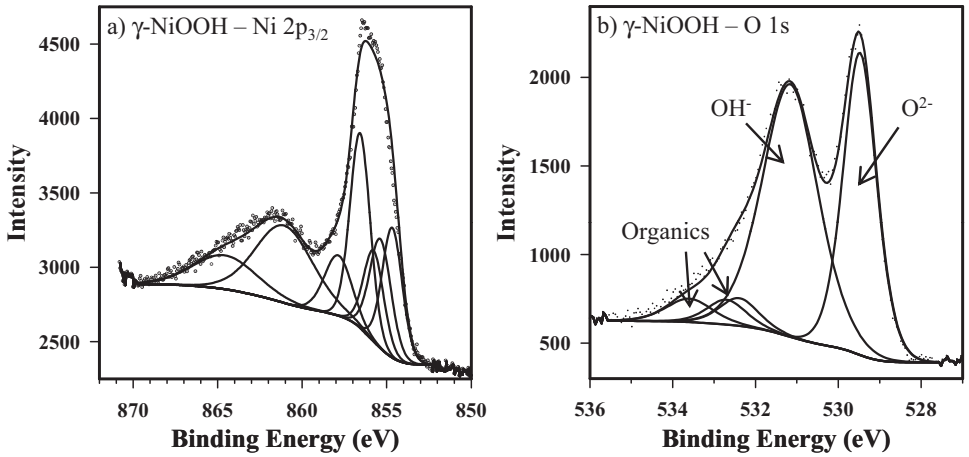

Fig. 3. Fitted high-resolution (a) Ni $2p_{3/2}$ and (b) O 1s spectra for γ-NiOOH powder. The Ni $2p_{3/2}$ spectrum was modelled using peak fit originally presented in reference [18]. The O 1s spectrum shows contributions from O^{2-} and OH− species along with additional intensity assigned to organic contamination at higher BE. The expected 1:1 O^{2-}:OH− peak area ratio is not observed here and suggests that the γ-NiOOH sample has started to decompose.

Fig. 2(a–d) contains the Ni $2p_{3/2}$ and O 1s spectra collected from two samples of the β-$Ni(OH)_2$ powder. Fitting of the respective O 1s spectra showed a strong peak representing bound hydroxide groups (OH^-) centred at either 530.8 eV or 530.9 eV depending on the sample (see Table 1) along with contributions from organic contamination at higher BEs. The O/Ni ratios were calculated and values of 2.0 were observed (see Table 2). To completely fit the O 1s spectrum shown in Fig. 2(d) an additional component at 531.5 eV was also required. The relative atomic contribution from this additional peak was not included in the atomic ratio calculations shown in Table 2 and this result indicated that this species was not chemically bound to any Ni^{2+} cations. We suggest that this species might result from interstitially positioned H_2O molecules within the layered brucite-like β-$Ni(OH)_2$ structure [37]. Three additional β-$Ni(OH)_2$ powder samples were analysed and the O/Ni ratios were found to range from 1.5 to 1.6. These may represent a structure that is undergoing degradation through loss of OH^-. The BE of the OH^- groups in this structure was found to be statistically higher (531.1 ± 0.1 eV) than in the hydroxides with the measured 2:1 O/Ni ratio (see Table 1). Representative high-resolution Ni $2p_{3/2}$ and O 1s

Table 2
Calculated O/M ratios using the normalised O, Ni, and Cr atomic concentrations in at%.

Sample	M $2p_{3/2}$		O 1s			O/M
	Ni or Cr species	at.%	O^{2-} at.%	O def at.%	OH^- at.%	
NiO-1	Ni^{2+}	38	28	11		1.0[a]
NiO-2		37	29	9.7		1.1[a]
NiO-3		38	30	8.6		1.0[a]
NiO-4		37	30	7.6		1.0[a]
$Ni(OH)_2$-1	Ni^{2+}	20			40	2.0
$Ni(OH)_2$-2		29			57	2.0
$Ni(OH)_2$-3		36			56	1.6
$Ni(OH)_2$-4		34			50	1.5
$Ni(OH)_2$-5		33			51	1.5
γ-NiOOH	Ni^{3+}	20	16		22	1.9[b]
$NiCr_2O_4$-1						
Ni	Ni^{2+}	10	40			4.0
Cr	Cr^{3+}	21				1.9
$NiCr_2O_4$-2						
Ni	Ni^{2+}	11	44			4.0
Cr	Cr^{3+}	23				1.9
Ni metal						
Ni metal	Ni^0	1.3				
NiO	Ni^{2+}	8.8	9.0			1.0[c]
$Ni(OH)_2$		10			20	2.0
NiCr metal						
Ni metal	Ni^0	0.9				
NiO	Ni^{2+}	1.6	1.6			1.0[c]
$Ni(OH)_2$		5.0			10	2.0
Cr metal	Cr^0	0.5				
Cr_2O_3	Cr^{3+}	1.8	2.7			1.5
$Cr(OH)_3$		4.1			13	3.2
Cr^{6+}	Cr^{6+}	0.4	1.2			3.0

[a] The O/Ni ratio was calculated using the combined atomic concentrations of the O^{2-} and O def species.
[b] The O/Ni ratio was calculated using the combined atomic concentration of the O^{2-} and OH^- species.
[c] The O/Ni ratio was calculated using the atomic concentration of the O^{2-} peak only. Based on the observed ratio there appeared to be no evidence to suggest that an O def species had formed.

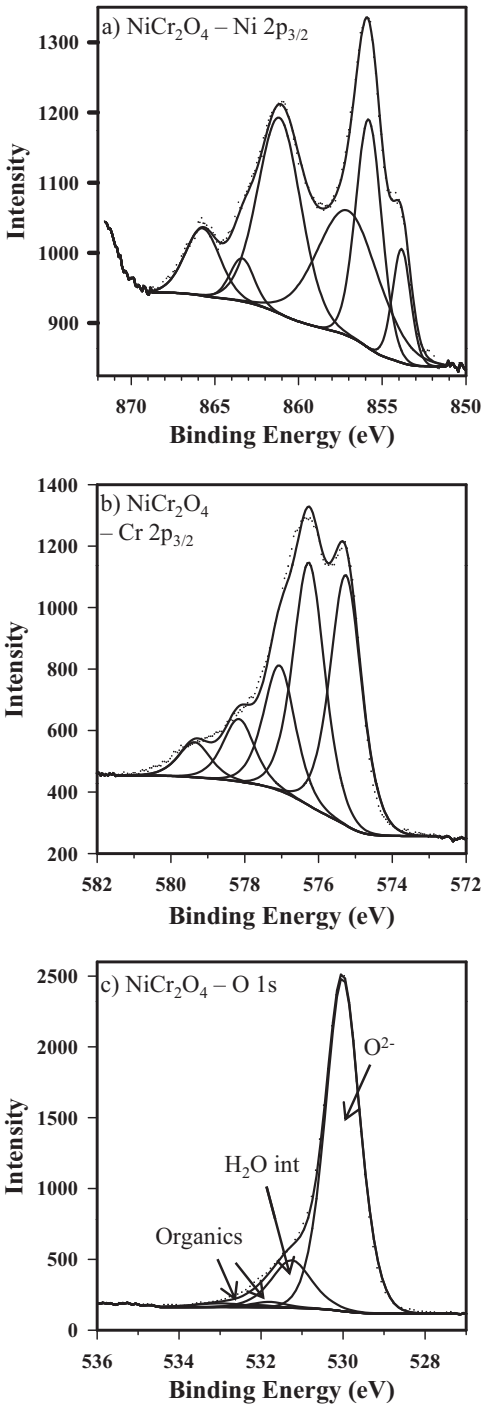

Fig. 4. Fitted high-resolution (a) Ni $2p_{3/2}$, (b) Cr $2p_{3/2}$ and (c) O 1s spectra for a powder sample of $NiCr_2O_4$. The high-resolution Ni $2p_{3/2}$ and Cr $2p_{3/2}$ spectra are shown with the fits presented in Refs. [1,19]. The O 1s spectrum shows the presence of lattice O^{2-} species along with small amounts of organic contamination. An additional peak was also required to completely fit the envelope and was assigned to H_2O int.

spectra for a OH^- deficient β-$Ni(OH)_2$ powder are shown in Fig. 2(e and f).

The Ni $2p_{3/2}$ and O 1s spectra collected from the γ-NiOOH powder are presented in Fig. 3. The O 1s spectrum was fitted with an O^{2-} component at 529.5 eV, an OH^- peak at 531.2 eV, along with contributions from organic contamination (see Table 1). An O/Ni ratio of 1.9 was obtained when the combined intensities of the OH^- and O^{2-} components were compared to the total Ni^{3+} concentration (see Table 2). Although this ratio is close to the expected value of 2, the 1:1 O^{2-}/OH^- ratio is not observed here. This suggests that the γ-NiOOH sample had started to decompose.

Fig. 4 contains representative Ni $2p_{3/2}$, Cr $2p_{3/2}$ and O 1s spectra collected from a powder sample of $NiCr_2O_4$. The O 1s spectra for both $NiCr_2O_4$ powders showed a strong component at either 529.9 eV or 530.0 eV attributed to lattice O^{2-}, a smaller peak located at 531.2 eV, and small contributions from organic material at higher BEs (see Table 1). The normalised Ni/Cr, O/Ni, and O/Cr ratios were found to be close to 2.0, 4.0, and 2.0, respectively (see Table 2). Thus the peaks at 529.9 eV and 530.0 eV represent all lattice O^{2-} sites within the inverse spinel structure and the small peak at 531.2 eV may be associated to the presence of interstitial H_2O molecules.

3.2. Aqueous reaction of metallic Ni and NiCr

The concept of using both peak shape and oxide ratio to identify and to estimate the relative proportions of mixed oxide systems, has been applied to some spectra produced during electrochemical oxidation of both polycrystalline Ni and NiCr alloy surfaces during simulation of solution conditions in PWR secondary coolant systems. Metallic Ni and NiCr alloy disks were subjected to 3 h aqueous exposures in a 0.0001 M LiOH solution (pH = 10 at 25 °C), at a constant potential of 1.5 V versus a 0.1 M Ag/AgCl reference electrode, and temperatures of 150 °C (Ni metal) and 25 °C (NiCr alloy) in a sealed autoclave. Following the aqueous reactions the metallic samples were removed from the autoclave and exposed to air prior to surface analysis. Modelling of the Ni $2p_{3/2}$ and Cr $2p_{3/2}$ spectra involved using different combinations of the fits presented in references [1,4,18–31,35] for metallic polycrystalline Ni, powdered polycrystalline NiO, β-$Ni(OH)_2$, γ-NiOOH, $NiCr_2O_4$, metallic Cr, powdered polycrystalline Cr_2O_3, $Cr(OH)_3{\cdot}xH_2O$, and CrO_3. Using the M $2p_{3/2}$ fitting results coupled with the expected O/M atomic ratios the corresponding O 1s peak areas for the O^{2-} and OH^- species were constrained. Contributions from any organic contaminates were estimated from the analysis of the C 1s high-resolution spectra and these intensities were then applied to the O 1s fit. The remaining spectral intensity was then attributed to the presence of interstitial H_2O molecules. From the XPS survey scans collected from both the Ni metal and NiCr alloy surfaces following aqueous oxidation a number of small impurities were also observed. The O 1s contribution of any possible oxide and or hydroxides associated with these species were assumed to be negligible and not included in the fit.

Fig. 5 shows the Ni $2p_{3/2}$ and O 1s spectra collected for the polycrystalline Ni metal surface. The Ni $2p_{3/2}$ spectrum was rigorously fitted using contributions from Ni metal (6.5%), NiO (44%), and β-$Ni(OH)_2$ (50%), while the analysis of the O 1s spectrum showed contributions from lattice O^{2-} at 529.2 eV, lattice OH^- at 531.1 eV and interstitial H_2O at 531.7 eV (see Table 1). The normalised O/Ni ratios calculated for the respective NiO and β-$Ni(OH)_2$ components were 1.0 and 2.0 (see Table 2). Thus, in this oxide/hydroxide composite there was no evidence for the O vacancy structure found for thin films of essentially single phase NiO [2,3]. While some higher oxidation states of Ni (i.e. in NiOOH) are predicted thermodynamically [38], no evidence for these was found: no Ni^{3+} line shape contributions are found and the O/Ni ratios are consistent with nearly equivalent concentrations of NiO and β-$Ni(OH)_2$.

Fig. 6(a–c) contains the high-resolution spectra collected from a NiCr surface following aqueous oxidation. The Ni $2p_{3/2}$ spectrum showed contributions from Ni metal (12%), NiO (21%) and β-$Ni(OH)_2$ (67%), while contributions from metallic Cr (7.6%) Cr_2O_3 (26%), $Cr(OH)_3$ (61%), and a fourth component attributed to a Cr^{6+} species (5.3%) were observed in the Cr $2p_{3/2}$ spectrum (see Table 1). Analysis of the O 1s spectrum showed signals at 529.3 eV (NiO), 529.5 eV (Cr_2O_3), 530.0 eV (Cr^{6+}-containing oxide), 531.2 eV

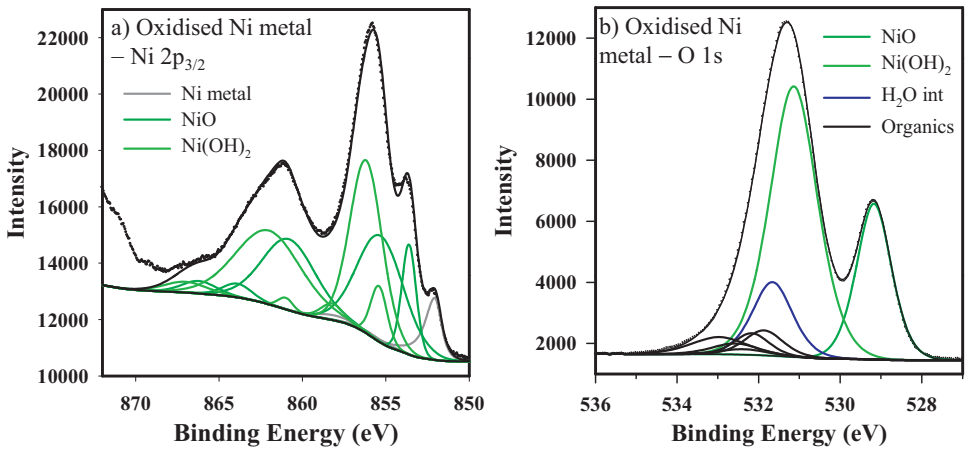

Fig. 5. Fitted high-resolution (a) Ni $2p_{3/2}$ and (b) O 1s spectra collected from a polycrystalline Ni metal disk subjected to aqueous oxidation. The Ni $2p_{3/2}$ spectrum showed contributions from metallic Ni, NiO and β-$Ni(OH)_2$. Fitting of the O 1s spectrum showed corresponding contributions from NiO, β-$Ni(OH)_2$, H_2O int, and organic contamination.

(β-$Ni(OH)_2$), and 531.3 eV ($Cr(OH)_3$). The corresponding normalised O/M ratios for the NiO, Cr_2O_3, β-$Ni(OH)_2$, and $Cr(OH)_3$ components were calculated to be 1.0, 1.5, 2.0, and 3.0 respectively, while the O/Cr ratio for the Cr^{6+}-containing oxide was found to be 3.0 (see Table 2). There was no evidence to support the formation of either NiOOH and or $NiCr_2O_4$ films on this surface. Two additional peaks at 530.2 and 531.8 eV were also required to fit the envelope. The higher BE species was attributed to interstitial H_2O associated with β-$Ni(OH)_2$, while the lower BE species is believed to result from interstitial H_2O molecules associated with $Cr(OH)_3$; according to our reassessment of O 1s spectral data for $Cr(OH)_3{\cdot}xH_2O$ originally shown in Ref. [35]. The normalised O/Cr atomic ratios for the

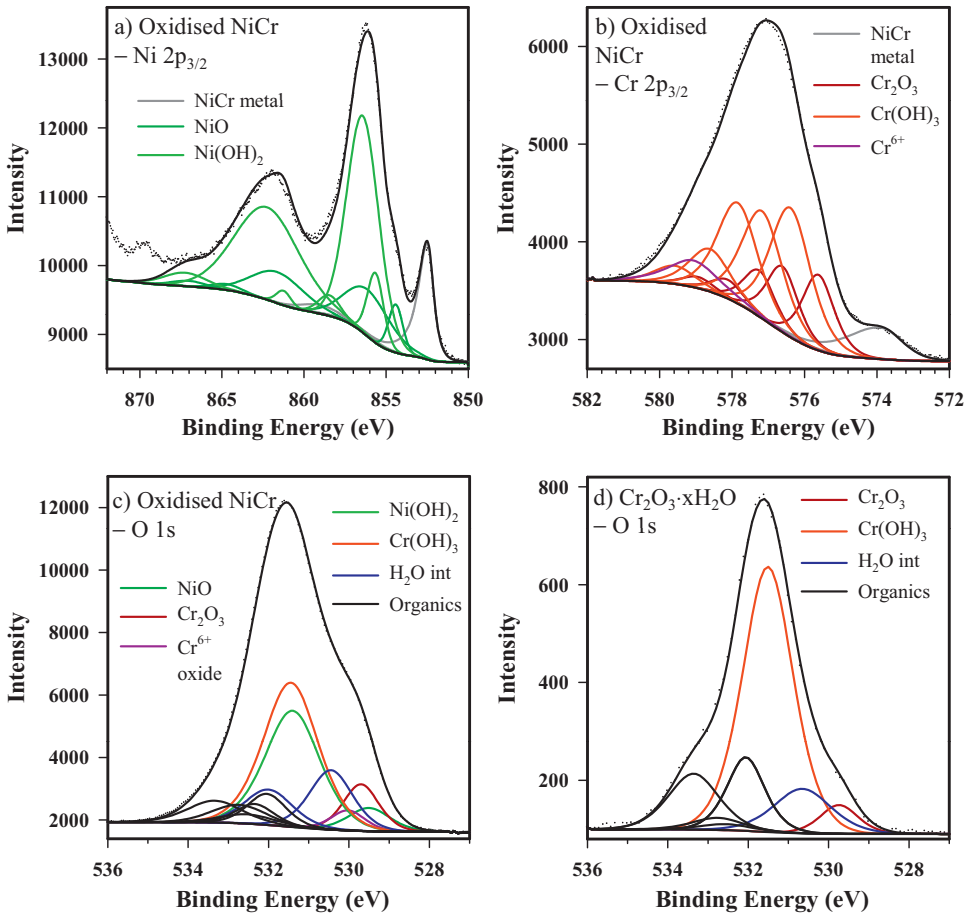

Fig. 6. Fitted high-resolution (a) Ni $2p_{3/2}$, (b) Cr $2p_{3/2}$, and (c) O 1s spectra collected form a NiCr disk subjected to aqueous oxidation. The Ni $2p_{3/2}$ spectrum showed contributions from metallic Ni, NiO and β-$Ni(OH)_2$. The Cr $2p_{3/2}$ spectrum was best fit with contributions from metallic Cr, Cr_2O_3, $Cr(OH)_3$, and a Cr6+-containing oxide. Fitting of the O 1s spectrum showed corresponding contributions from NiO, Cr_2O_3, a Cr6+-containing oxide, β-$Ni(OH)_2$, and $Cr(OH)_3$. Two additional components representing H_2O int species associated with both β-$Ni(OH)_2$ and $Cr(OH)_3$ were also observed. The remainder of the O 1s intensity was determined to result from organic contamination.

Cr_2O_3 and $Cr(OH)_3$ components were calculated to be 1.5 and 3.0, respectively. The re-fitted O 1s spectrum for $Cr(OH)_3{\cdot}xH_2O$ is shown in Fig. 6(d).

4. Conclusion

The corrected O/Ni atom ratios were determined for powder samples of polycrystalline NiO, β-$Ni(OH)_2$, γ-NiOOH, and $NiCr_2O_4$ and were shown to correspond well to the expected atom ratios for these oxides. For some particular samples of β-$Ni(OH)_2$ and γ-NiOOH, the O/Ni ratios suggested that the sample was decomposing. The O/Ni and O/Cr ratios were then used to confirm the assignments of mixed oxide phases that formed on Ni metal and NiCr alloy surfaces during electrochemical oxidation.

Acknowledgements

The authors thank Professor David Shoesmith for the use of the electrochemical equipment in his laboratory. Additional thanks are extended to Dr. Pellumb Jakupi and Dr. Jamie Noël for their help in completing the aqueous oxidation experiments. The financial support of NSERC is also warmly acknowledged.

References

[1] M.C. Biesinger, B.P. Payne, A.P. Grosvenor, L.W.M. Lau, A.R. Gerson, R.St.C. Smart, Appl. Surf. Sci. 257 (2011) 2717.
[2] B.P. Payne, M.C. Biesinger, N.S. McIntyre, J. Electron Spectrosc. Relat. Phenom. 175 (2009) 55.
[3] B.P. Payne, A.P. Grosvenor, M.C. Biesinger, B.A. Kobe, N.S. McIntyre, Surf. Interface Anal. 39 (2007) 582.
[4] M.C. Biesinger, B.P. Payne, L.W.M. Lau, A.R. Gerson, R.St.C. Smart, Surf. Interface Anal. 41 (2009) 324.
[5] M.W. Roberts, R.St.C. Smart, J. Chem. Soc. Faraday Trans. 80 (1984) 2957.
[6] M.W. Roberts, Surf. Sci. 299/300 (1994) 769.
[7] A.F. Carley, P.R. Chalker, M.W. Roberts, J. Chem. Soc. Chem. Commun. 80 (1984) 459.
[8] A.F. Carley, S. Rassias, M.W. Roberts, Surf. Sci. 135 (1983) 35.
[9] P.R. Norton, R.L. Tapping, J.W. Goodale, Surf. Sci. 65 (1977) 13.
[10] C. Benndorf, C. Nöble, F. Thieme, Surf. Sci. 121 (1982) 249.
[11] J.M. Heras, E.V. Albano, Appl. Surf. Sci. 17 (1983) 207.
[12] J.M. Heras, E.V. Albano, Appl. Surf. Sci. 17 (1983) 220.
[13] N.S. McIntyre, R.D. Davidson, T.L. Walzak, A.M. Brennenstuitl, F. Gonzalez, S. Corazza, Corros. Sci. 37 (1995) 1059.
[14] N.S. McIntyre, D.G. Zetaruk, D. Owen, J. Electrochem. Soc., Electrochm. Soc. 126 (1979) 750.
[15] N.S. McIntyre, T.E. Rummery, M.G. Cook, D. Owen, J. Electrochem. Soc., Electrochem. Soc. 123 (1976) 1164.
[16] A. Machet, A. Galtayries, S. Zanna, L. Klein, V. Maurice, P. Jolivet, M. Foucault, P. Combrade, P. Scott, P. Marcus, Electrochim. Acta 49 (2004) 3957.
[17] A. Machet, A. Galtayries, P. Marcus, P. Combrade, P. Jolivet, P. Scott, Surf. Interface Anal. 34 (2002) 197.
[18] A.P. Grosvenor, M.C. Biesinger, R.St.C. Smart, N.S. McIntyre, Surf. Sci. 600 (2006) 1771.
[19] D. Alders, F.C. Voogt, T. Hibma, G.A. Sawatzky, Phys. Rev. B 54 (1996) 7716.
[20] S. Altieri, L.H. Tjeng, A. Tanaka, G.A. Sawatzky, Phys. Rev. B 61 (2000) 13403.
[21] M.L. Burke, D.W. Goodman, Surf. Sci. 311 (1994) 17.
[22] S.C. Street, C. Xu, D.W. Goodman, Annu. Rev. Phys. Chem. 48 (1997) 43.
[23] M. Bäumer, D. Cappus, G. Illing, H. Kuhlenbeck, H.-J. Freund, J. Vac. Sci. Technol. A 10 (4) (1992) 2407.
[24] D. Cappus, C. Xu, D. Ehrlich, B. Dillmann, C.A. Ventrice Jr., K. Al Shamery, H. Kuhlenbeck, H.-J. Freund, Chem. Phys. 177 (1993) 533.
[25] D. Cappus, M. Menges, C. Xu, D. Ehrlich, B. Dillmann, C.A. Ventrice Jr., J. Libuda, H.-J. Freund, J. Electron Spectrosc. Relat. Phenom. 68 (1994) 347.
[26] St. Uhlenbrock, C. Scharfschwerdt, M. Neumann, G. Illing, H.-J. Freund, J. Phys.: Condens. Matter 4 (1992) 7973.
[27] M.A. Langell, C.L. Berrie, M.H. Nassir, K.W. Wulser, Surf. Sci. 320 (1994) 25.
[28] M.A. Langell, M.H. Nassir, J. Phys. Chem. 99. (1995) 4162.
[29] A.F. Carley, P.R. Chalker, M.W. Roberts, Proc. R. Soc. Lond. A 399 (1985) 167.
[30] A.F. Carley, M.W. Roberts, Proc R. Soc. Lond. A 363 (1978) 403.
[31] M.C. Biesinger, C. Brown, J.R. Mycroft, R.D. Davidson, N.S. McIntyre, Surf. Interface Anal. 36 (2004) 1550.
[32] N. Fairley, CasaXPS Version 2.2.15, 1999–2009.
[33] C.D. Wagner, L.E. Davis, M.V. Zeller, J.A. Taylor, R.M. Raymond, L.H. Gale, Surf. Interface Anal. 3 (1981) 211.
[34] C.D. Wagner, J. Electron Spectrosc. Relat. Phenom. 32 (1983) 99.
[35] B.P. Payne, M.C. Biesinger, N.S. McIntyre, J. Electron Spectrosc. Relat. Phenom. 184 (2011) 2717.
[36] G. Beamson, D. Briggs, High-resolution XPS of Organic Polymers. The Scienta ESCA300 Database, John Wiley and Sons, Toronto, 1992 (Appendices 1–3).
[37] C. Delmas, C. Faure, L. Gautier, L. Guerlou-Demourgues, A. Rougier, Philos. Trans. R. Soc. Lond. A 354 (1996) 1545.
[38] B. Beverskog, I. Puigdomenech, Corros. Sci. 39 (1997) 969.